Kejalakshmy, N., Rahman, B. M., Agrawal, A., Tanvir, H. M. & Grattan, K. T. (2009). Metal-Coated Defect-Core Photonic Crystal Fiber for THz Propagation. IEEE/OSA Journal of Lightwave Technology, 27(11), 1631 - 1637. doi: 10.1109/JLT.2009.2020919 <http://dx.doi.org/10.1109/JLT.2009.2020919>

Metal-coated defect-core photonic crystal fiber for THz propagation

N. Kejalakshmy, B. M. Azizur Rahman, *Senior Member, IEEE*, A. Agrawal, H. Tanvir, and K. T. V. Grattan

***Abstract*— Modal solutions for metal-coated defect-core photonic crystal fiber (PCF) with a central air-hole have been obtained by using a full-vectorial finite element method to model the guidance of THz waves. It has been shown that the surface plasmon modes can couple with the defect-core PCF mode to form supermodes, with potential for sensing applications.**

***Index Terms*—Finite Element method (FEM), Holey fiber, Modal solutions, Surface Plasmon.**

I. INTRODUCTION

PHOTONIC crystal fiber (PCF) is a microstructured optical waveguide with low index air-holes running parallel to and along the length of the optical fiber [1]. Various structural variations of PCF designs have been considered to obtain a higher birefringence, for nonlinear applications, band gap modifications and their tailored dispersion properties [1]. Recently polymer based PCF has also been demonstrated to guide terahertz waves (THz) [2, 3]. In this article the modal properties of a metal-coated defect-core PCF with an air-hole at the center are reported by using a full-vectorial finite element method (FEM) [4]. Recently PCF designs supporting a surface plasmon mode (SPM) using the metal-coatings in the cladding region have been reported, designed for their applications in the optical frequencies [5-8]. In this study, metal is introduced in the central air-hole of a defect-core PCF in order to influence the modal properties significantly in the THz domain, studying their guidance properties for a range of potential applications, including evanescent sensing [9]. The structure suggested here is feasible for fabrication with available technologies: involving the deposition of metal-coatings on the microstructured fibers [10], fabrication technology using Teflon to create the PCF [3], techniques for copper coating on Teflon using Chemical Vapor Deposition [11] and metal-coated hollow waveguide technology [12]. Through tailoring the design of a PCF, it is possible to allow the coupling (which is tunable by varying the size of air-holes) between the SPMs at the metal-coated interface and the fundamental mode of a defect-core PCF (DCPCF). The modal properties may be analyzed by using a full-vectorial FEM, proven successful in the analysis of SPM in metal-coated hollow waveguides [13]. In the present analysis a full-vectorial, complex **H** field-based method with a penalty function and perfectly matched layer (PML) boundary conditions has been applied for the modal analysis of metal-coated central air-hole in a defect-core PCF (MCDCPCF).

Manuscript received November 10, 2008. This work was supported by the European Community's Sixth Framework Programme under the Marie Curie Intra-European Fellowships (Contract MEIF-CT-2005-025339) and UKIERI. The authors are with the City University, School of Engineering and Mathematical Sciences, Northampton Square, London EC1V 0HB, UK, (phone: +44-20-70408123; fax: +44-20-70408568; e-mail: B.M.A.Rahman@city.ac.uk).

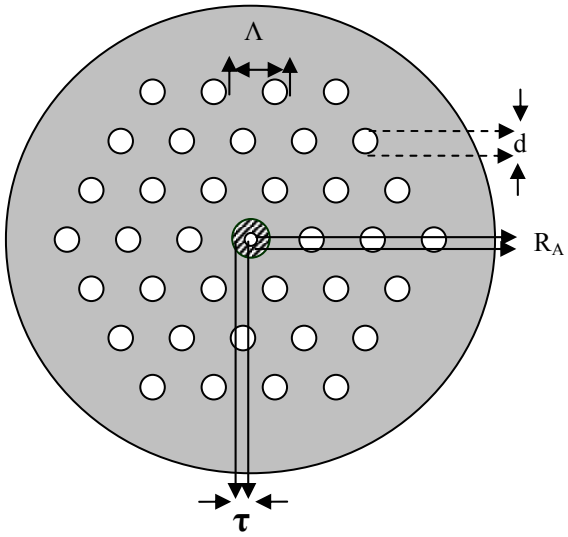

Fig. 1 Cross section of a metal-coated defect-core PCF.

In the modal solution approach based on the FEM, the intricate cross section of a PCF can be represented by using many triangles of different shapes and sizes. This flexibility makes the FEM preferable when compared to finite difference methods which not only use inefficient regular spaced meshing, but also cannot represent slanted or curved dielectric interfaces. The modes in high index contrast PCF, with two-dimensional confinement, are also hybrid in nature, with all six components of the **E** and **H** fields being present. Hence only a full-vectorial characterization can accurately be used to determine their modal solutions. In the present approach, a **H**-field based rigorous full-vectorial FEM has been used to analyze a metal coated defect-core PCF operating at 1.0 THz.

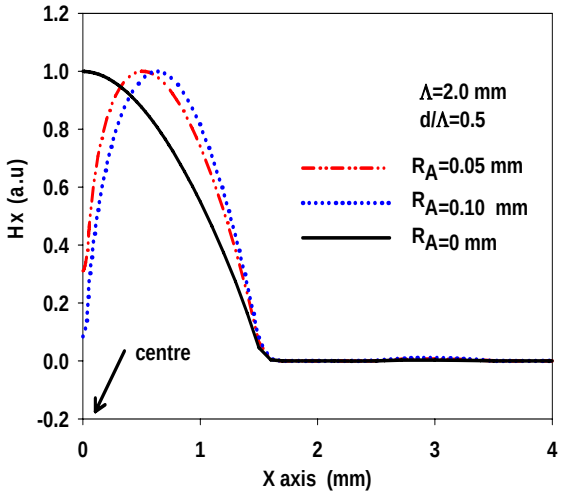

Fig.2. H^x_{11} mode for different defect hole radii R_A=0.0, 0.5, 0.1 mm for DCPCF without metal coating.

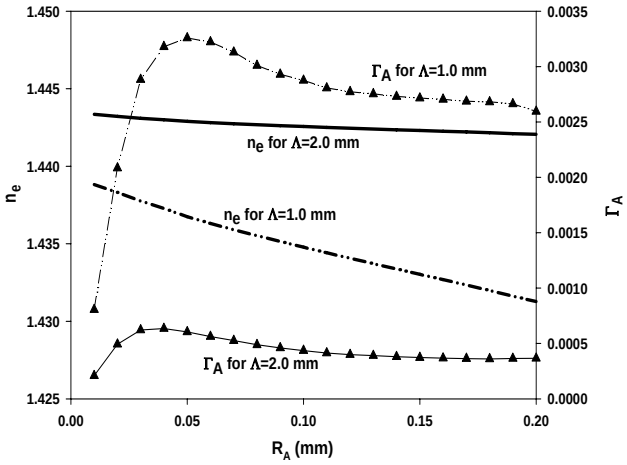

Fig.3. Variation of the confinement factor and effective index of the H^x_{11} mode with the central air-hole radius R_A.

II. Result

A. Propagation in a PCF with Central Air-Hole Defect

The PCF design discussed here represents a holey microstructured fiber created from Teflon with a central air-hole defect. Figure 1 represents the cross-section of such a PCF with a metal-coated central air-hole. The complex refractive index of Teflon is considered to be 1.445 + *j* 0.00119 [14, 15] at 1.0 THz. The material cross section is accurately represented where all the air-holes are arranged in the triangular lattice, with the pitch length, Λ, being the distance between the air-holes and 'd' the diameter of all the air-holes (except the central one). The radius of the central air-hole is R_A. Here the central air-hole has a metal coating of thickness τ. In the illustration, the background material shaded in the gray color represents the Teflon. A cladding region with three air-hole rings has been considered in this rigorous evaluation of the PCF design.

Initially the modal properties of a defect-core PCF without a metal coating (τ=0) are studied. The H_x fields of the fundamental quasi-TM (H^x_{11}) mode of this PCF at 1 THz (with τ=0, d/Λ=0.5, Λ=2.0 mm) for three different radii, R_A = 0, 0.05 and 0.01 mm are shown in Fig. 2. The field profile shown by a solid line is nearly Gaussian shaped when R_A is zero (without a defect-central air-hole). However, as R_A increases, the field deviates rapidly from the Gaussian profile with a dip in the center of the core, showing a profound effect for even a smaller R_A. It can be seen in Fig. 2, when R_A=0.05 mm the field dips to 30% of the peak value (shown by a chained line) and when R_A=0.10 mm (shown by dotted line) the field is reduced to only 8% of the maximum value. When R_A=0.2 mm, not shown here, the power confinement factor in the central air-hole Γ_A is only 0.0003, while with the air-holes in the cladding region, $\Gamma_{clad} \approx 0.0004$ and most of the remaining power is in the Teflon. Here the Pyonting vector was calculated from the **H**-field and this energy flux density may be integrated to obtain the power confinement factor in a particular region. The spot-size area for this case is around 7.0 mm^2 and the spot-size may be calculated by integrating the area with a field intensity higher than $1/e^{th}$ of its highest value.

Figure 3 shows the variations of effective index and the confinement factor with the R_A for Λ=1.0 and 2.0 mm. The effective index is lower for a smaller pitch, Λ=1.0 mm, as the mode is more exposed to the cladding air-holes, compared to that of the larger pitch value. The effective indices also decrease with R_A as the equivalent index of the core reduces due to the enlarged central air-hole. It can also be observed that the rate of change is more profound for the smaller pitch length, as the mode is less confined for the smaller waveguide dimension. The confinement factor, Γ_A, initially increases with the R_A, and reaches a maximum value. With a further increase of R_A, the confinement factor Γ_A decreases, accompanied by an associated increase in the Γ_{clad}. As result, the modal loss starts to increase until the mode reaches a cut-off value, at around $R_A \leq d/2$. When R_A=d/2, the central defect air-hole is identical to the other air-holes; the structure becomes fully periodic without defects present and such a uniform medium without any defect cannot support a mode. It can also be observed that the value of Γ_A is large for the smaller pitch values, as the tightly packed air-holes lead to higher power confinement in the air-holes.

B. Metal Coated Central Air-Hole

Previously research on the excitation of SPMs has been reported in PCF where metal-coated channels and metal rods were introduced into the cladding region [5-8] and operation

at optical frequencies was considered. In this study, it is shown that the SPMs can couple with the mode of a defect-core PCF with a central air-hole, when the metal-coating is deposited around this central air-hole. The coating here has been assumed to be copper, whose real and imaginary parts of the refractive index are taken as 438 and 494, respectively [16] at 1.0 THz.

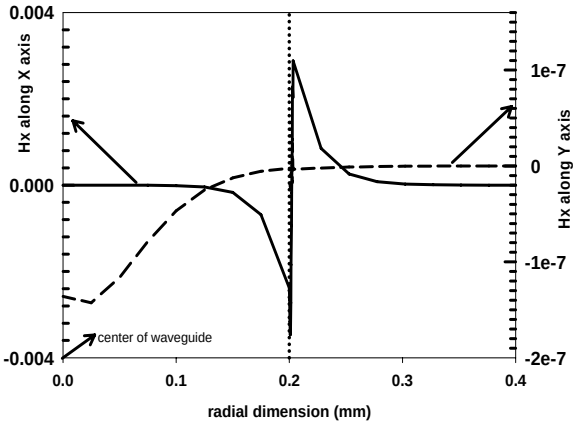

Fig. 4. H_x field profile of the SPM1 mode for Λ=2.0 mm, d/Λ=0.5, R_A=0.2 mm, τ=0.0034 mm. Dotted line represents the position of metal. The solid line represents the H_x along X axis and the dashed line represents Y axis.

It is well known that a SPM can form at a single metal/dielectric interface and for a thin metal layer bounded by two dielectrics, these two SPMs at the two interfaces couple to form two supermodes when the metal thickness is small [17]. The first supermode, SPM1, is an odd-type with its higher effective index value and the second one, SPM2, with a lower effective index value is the even-type supermode. The SPM1 at the Teflon/metal/air interfaces of the metal-clad air-hole shown in Fig. 4, is also known as the short-range mode which has a higher modal loss than the second supermode. The variations of the H_x field along the x- and y-axes are shown by a solid and dashed line, respectively. This SPM with the dominant H_x value is only formed at the metal interfaces along the x-direction at x= ±0.2 mm = R_A. The field shape is similar to a typical odd-type or 'short-range' SPM [17] which forms at both the interfaces along the x-axis. The magnitude of the H_x field is very small along the y-axis but with a different spatial variation. A similar SPM, but with the dominant H_y field is supported at the two metal/dielectric interfaces along the y axis (but not shown here). The central air-hole has a power confinement factor Γ_A = 0.49. This mode is highly localized and its effective area A_{SMI} is 0.25 mm^2, where A_{SMI} is the effective area based on the second moment of the intensity distribution [18] and this definition is considered here as the field profile of this SPM1 differs significantly from a Gaussian shape. This mode has a much higher effective index than the core mode of the PCF and does not interact with it and is not considered further in this work.

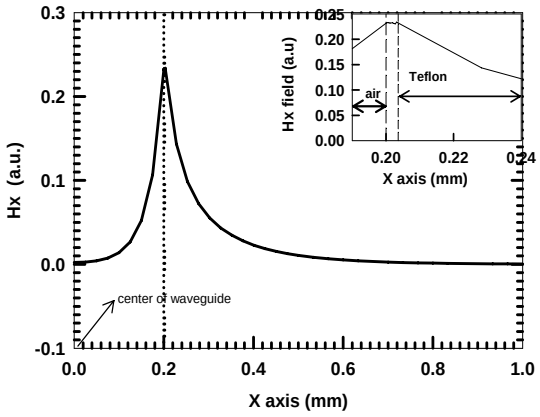

(a)

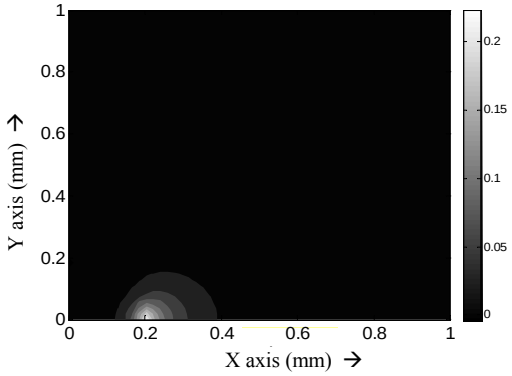

(b)

Fig. 5. H_x field of the SPM2 mode for Λ=2.0 mm, d/Λ=0.5, R_A=0.2 mm, τ=0.0036 mm. (a) H_x field variation along X-axis. Dotted line represents the position of metal. The inset shows the variation of the field near the metal coating and the region between the dashed lines represents metal. (b) H_x field contour plot.

The variation of the H_x field for the SPM2, is shown in Fig. 5 for a PCF with parameters Λ=2.0, R_A=0.2 mm, τ=3.6 μm. A contour plot of this mode is shown in Fig. 5(b). This SPM with the dominant H_x field is formed at the Teflon/copper/air interfaces, but the field profile of this mode is similar to that of a typical even-type 'long-range' SPM [12]. The variation of the H_x field along the x-axis is shown in Fig. 5(a). It can be observed that the field profile decays quickly in the bounding air region on the left and more slowly in the Teflon layer on the right. There is a small dip inside the thin metal layer (shown as an inset), typical of an even-type SPM. It is also clear that two even-type SPMs at the left and right (x=±0.2 mm) Teflon/copper/air interfaces of the metal-clad air-holes are coupled to form this SPM2 supermode. The SPM2 is highly lossy and the loss value increases with the metal thickness, similar to an even-type SPM in optical waveguide [17]. Here the material loss for both the Teflon and copper has

been included along with the leakage loss of this PCF. The modal confinement of the mode SPM2 can be controlled by varying the metal thickness and this has a power confinement factor in the central air-hole with $\Gamma_A \approx 0.40$-0.60 while the remaining power is distributed in the Teflon. This mode, with a lower effective index value, can couple to the dielectric mode of the PCF core and will be investigated further.

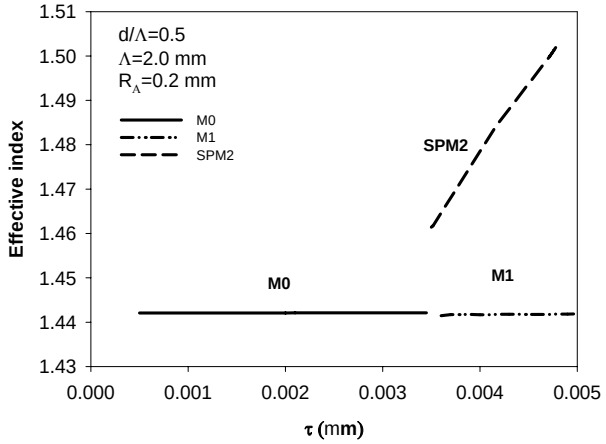

Fig. 6 (a). The variation of effective index of the M0, M1 and SPM2 modes for Λ=2.0 mm, d/Λ=0.5, R_A=0.2 mm.

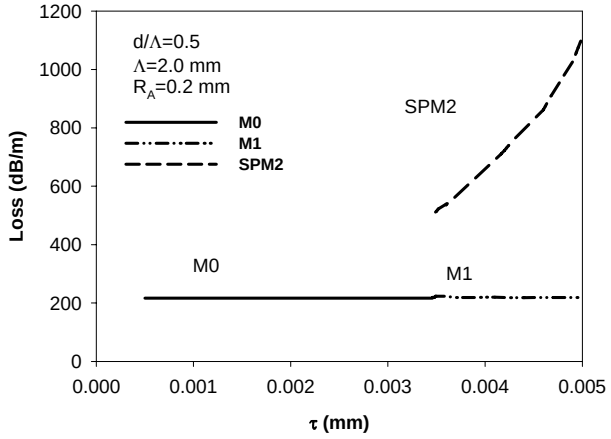

Fig. 6(b). Variation of leakage loss of the M0, M1 and SPM2 modes for Λ=2.0 mm, d/Λ=0.5, R_A=0.2 mm.

Variations of the effective indices and loss values for several modes are shown in Figs. 6(a) and 6(b). The first supermode, SPM1, whose effective index and modal loss are very high ($n_e \approx 2.4$, loss≈3000dB/m around τ=3.0μm), is not considered here, but its field profile is shown in Fig. 4. The field profile of the second SPM2 is also shown in Fig. 5. Figure 7 shows the H_x field variation along the x-axis for the core mode, M0. When the metal thickness is small, the

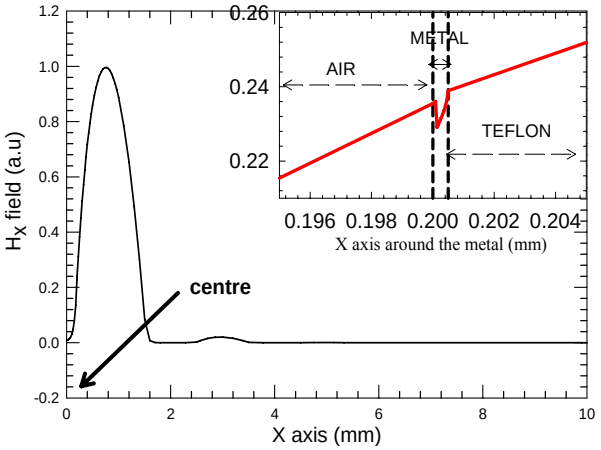

Fig. 7. Variation of the H_x field along the X-axis for the M0 mode when τ=0.0005 mm, Λ=2.0 mm, d/Λ=0.5, R_A=0.2 mm. The inset shows the variation of the field near the metal coating and the region between the dashed lines represents metal.

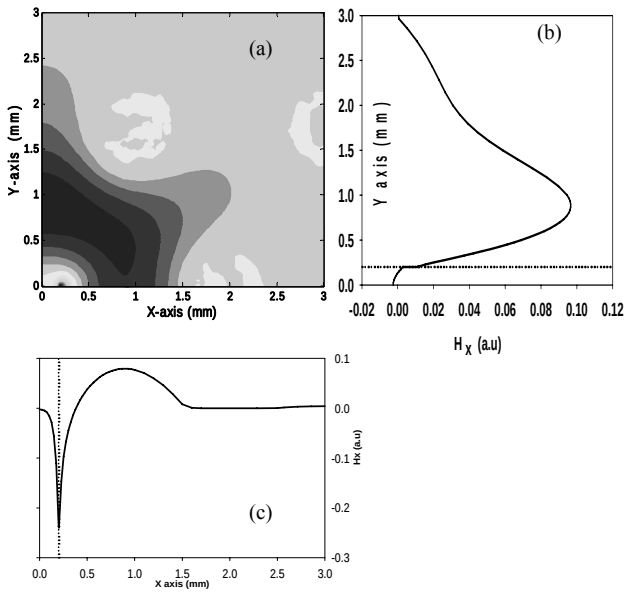

Fig. 8. H_x field profile of M1 mode modes for Λ=2.0 mm, d/Λ=0.5, R_A=0.2 mm, τ=0.0036 mm. (a) The upper left diagram corresponds to the contour field profile. (b) The upper right line plot corresponds to the variation of H_x field along the Y axis. (c) The lower line plot corresponds to the variation H_x field along the X axis. Dotted line represents the position of metal.

dominant H_x field of the M0 mode is similar to that of the DCPCF mode shown in Fig.2 for an uncoated PCF (τ=0), but the figure clearly shows a small perturbation of the field across the thin metal layer (in the inset). As the metal thickness increases, the effective index increases, but this change is very small. Although the structure processes six-fold rotational symmetry, the field along y-axis spreads more

in the cladding region compared to the field along the x-axis, which is characteristic of a DCPCF mode and as well as that of a PCF mode, which is due to the position of the six air-holes in the first ring, nearest to the core. The power confinement factor in the Teflon (Γ_T) is around 0.998 and the central air-holes possess only 0.0005 of the total power. The effective area remains nearly constant – similar to that of an uncoated DCPCF (τ=0) (not shown here). It can be observed that as the metal thickness is reduced the effective index of the SPM2 reduces and below its cutoff thickness this structure cannot support this mode. However, when the effective index of this odd SPM2 approaches the effective value of the DCPCF mode near τ = 3μm, their interaction converts the M0 mode to M1 mode.

When τ> 3.0 μm, two modes are of particular interest, these being SPM2 and M1, as their interactions can be used for several sensing applications. Variations of the effective indices and loss values of these two modes were shown in Figs. 6(a) and 6(b) respectively. The modal loss and the effective index of M1 mode is nearly the same as the M0 mode, while the SPM2 mode has a higher loss value than the M1 mode.

The variation of the H_x field for the M1 mode for τ= 3.6 μm is shown in Fig. 8. For clarity, only one-quarter of the waveguide structure is shown in Fig. 8(a), where a sharp peak field exists along the x-axis at the metal/air interface of the central air-hole, only visible as a 'dot' but this is clearly seen from the lower line diagram in Fig. 8 (c). This lower line diagram has a dotted line to show the position of the metal layer at x=0.2 mm along the x-axis. Similarly, the right-side line diagram has a dotted line at y=0.2 mm along the y-axis to locate the metal coating, where the field is forced to zero due to the boundary conditions. The field in the PCF core follows typical six-fold star shape, except near the metal interface. For this mode, since the field profile changes its sign along the x-axis, as is clearly shown in Fig. 8 (c), it can be considered as a higher order mode. Since most of the field is distributed in the Teflon core, except for the sharp peak at the metal interface, the effective index of this mode is close to that of M0. Away from the metal-coated central air-hole, the field shows the characteristic of a typical DCPCF mode.

C. EFFECT OF VARYING THE PITCH

The phase matching between the DCPCF mode and a SPM can be varied by adjusting the geometrical parameter of a DCPCF. Fig. 9(a) shows the contour profile of the M0 mode and Figs. 9(b) and 9(c) show the H_x field profile along the X and Y axes for Λ=1.0 mm, d/Λ=0.5, R_A=0.1 mm with τ=3.3μm. H_x has the same sign in the air-hole and Teflon core region. In this case, Γ_A is about 0.01 and the field value falls to 10% of its maximum value. It can be noted that in this case the changes in the pitch value and the central air-hole radius modified by the field profile significantly.

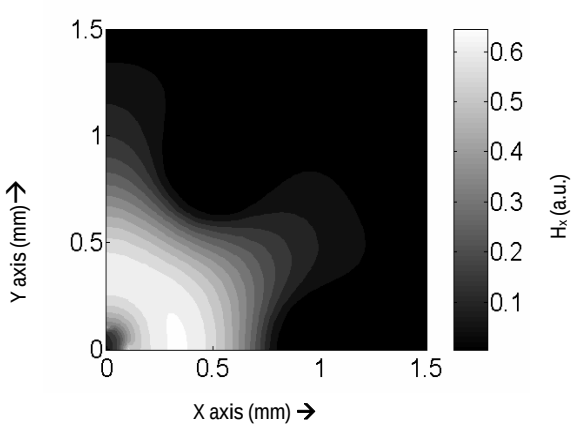

(a)

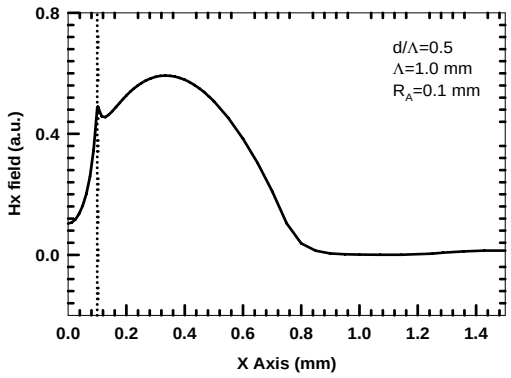

(b)

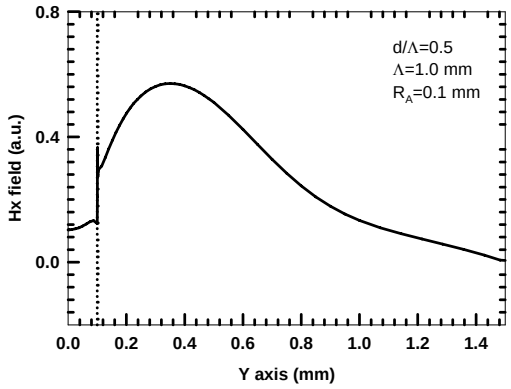

(c)

Fig.9. (a) Contour profile of Hx field for M0 mode with Λ=1.0mm, d/Λ=0.5, R_A=0.1mm, τ=0.0033 mm. (b) The variation H_x field along the X axis. (c) The variation H_x field along the Y axis. The dotted lines in (b) and (c) represent the position of metal.

This M0 mode has most of its power confinement (Γ_T=0.98) in the Teflon region. However the power

confinement in the central air-hole in this M0 mode is ten-fold greater than that of the M0 mode shown in Fig.7. This again suggests that the DCPCF mode has coupled more strongly with the SPMs. As a result, the power confinement in the central air-hole (Γ_A) can be influenced by varying the air-filling fraction in the cladding and by the presence of a sensing medium. For this mode, the effective area A_{SMI} is around 8 mm^2.

D. EFFECT OF AIR-FILLING FRACTION

In the next study, the variation of the Γ_A for the M1 mode with the air-filling fraction (d/Λ=0.5-0.9) is shown in Fig. 10 for two different pitch values, Λ=1.5 mm (dashed–dotted line) and 2.0 mm (dashed line). In this case, the metal thickness is kept constant at τ=0.36 μm. When d/Λ is increased, the effective index of the mode decreases as the field is more exposed to the larger air-holes. The corresponding variations of effective indices are shown by circle and triangular symbols for pitch values of 2.0 mm and 1.5 mm respectively. By increasing the air-filling fraction, the power distributed in the Teflon can be reduced, with a corresponding increase in Γ_A. For the range considered here the power confinement factor in Teflon material decreases from 0.99 to 0.9. However by increasing d/Λ from 0.5 to 0.9, the total loss value increases from 220 dB/m to 235 dB/m because the power confinement factor increases inside the metal region (this is not shown here).

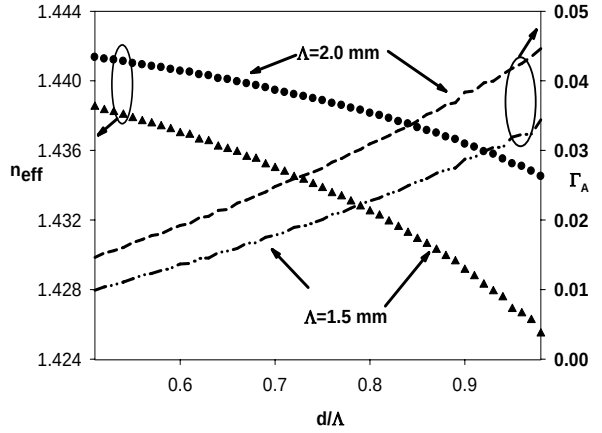

Fig. 10. Variation of effective index and Γ_A of the mode M1 with d/Λ, when Λ=2.0 and 1.5 mm, R_A=0.2mm, τ=0.0036 mm.

III. CONCLUSION

For the first time, the modal properties of coupled surface plasmon and dielectric modes in a metal-coated central air-hole PCF are reported, obtained by using a rigorous **H**-field finite element method. In this case, a single central air-hole would allow its modal properties to be controlled better by the presence of a sensing medium in this region and this can be further enhanced by using a metal-coating in this air-hole. Different mode profiles from pure dielectric and SPMs to the coupled SPMs are shown to exist in such structures. In the present configuration, it has been shown that the SPM can couple with a DCPCF mode by use of the metal-coating of a single air-hole. The power fraction, the modal indices, and the modal loss can be easily controlled by the waveguide parameters. The metal coated DCPCF can potentially find a variety of applications in the THz region, in PCF designs created by introducing a sensing material in the central hole or in sensing a bio-molecule [19, 20] adjacent to the metal layer.

REFERENCES

[1] P. St. J. Russell, 'Photonic-Crystal Fibers,' J. Lightwave Technol. **24**, 4729-4747 (2006).

[2] H. Han, H. Park, M. Cho and J. Kim, 'Terahertz pulse propagation in a plastic photonic crystal fiber,' Appl. Phys. Lett. **80**, 2634-2636 (2002).

[3] M. Goto, A. Quema, H. Takahahi, S. Ono, and N. Sarukura, 'Teflon photonic crystal fiber as terahertz waveguide,' Jpn. J. Appl. Phys, Part 2 **43**, L317-L319(2004).

[4] B. M. A. Rahman and J. B. Davies, 'Finite-element solution of integrated optical waveguides,' J. Lightwave Technol. **2,** 682-688 (1984).

[5] M. Hautakorpi, M.Mattinen and H Ludvigsen, 'Surface-plasmon-resonance sensor based on three-hole microstructured optical fibre,' Opt. Express **16,** 8427-8432 (2008).

[6] B. T. Kulmey, K. Pathmanandavel and R.C. McPhedran, 'Multipole analysis of photonic crystal fibers with coated inclusion,' Opt. Express **14**, 10851-10864 (2006).

[7] J. Hou, D. Bird, A. George, S. Maier, B. T. Kuhlmey and J. C. Knight, 'Metallic mode confinement in microstructured fibres,' Opt. Express **16**, 5983-5990 (2008).

[8] A. Hassani and M. Skorobogatiy, 'Design criteria for microstructured-optical fiber based surface-plasmon-resonance sensors,' JOSA B **24**, 1423-1429 (2007).

[9] A. Hassani and M. Skorobogatiy, 'Surface plasmon resonance-like integrated sensor at terahertz frequencies for gaseous analytes,' Opt. Express **16**, 20206-20214 (2008).

[10] P.J.A. Sazio, A. Amezcua-Correa, C.E. Finlayson, J.R. Hayes, T.J. Scheidemantel, N. F. Baril, B. R. Jackson, D. J. Won, F. Zhang, E.R. Margine, V. Gopalan, V.H. Crespi, and J.V. Badding, 'Microstructured optical fibers as high pressure microfluidic reactors,' Science **311,** 1583-1586 (2006).

[11] T. Y. Chen, C. Combellas, P. Doppelt, F. Kanoufi, A. Thiébault, 'Selective Metallization of Mg/NH3-Treated Teflon by Copper CVD,' Chemical Vapor Deposition **5**, 185 – 190 (1999).

[12] J. A. Harrington, R. George, P. Pederson and E. Mueller, 'Hollow polycarbonate waveguides with inner Cu coatings for delivery of terahertz radiation,' Opt. Express **12**, 5263-5268 (2004).

[13] C. Themistos, B. M. A. Rahman, M. Rajarajan, K. T. V. Grattan, B. Bowden, and J. A. Harrington, 'Characterization of Silver/Polystyrene (PS)-coated hollow glass waveguides at terahertz frequency,' J. Lightwave. Technol. **25**, no. 9, September 2007.

[14] Y. S. Jin, G. J. Kim and S. G. Jeon, 'Terahertz Dielectric Properties of Polymers,' Jrnl. Korean Physical Society **49**, 513-517 (2006).

[15] C. Winnewisser, F. Lewen and H. Helm, 'Transmission characteristic of dichroic filters measured by THz time domain spectroscopy,' Appl. Phys. A. **66**, 593-598 (1998).

[16] M. A. Ordal, R. J. Bell, R. W. Alexander, Jr., L. L. Long, and M. R. Querry, 'Optical properties of fourteen metals in the infrared and far infrared: Al, Co, Cu, Au, Fe, Pb, Mo, Ni, Pd, Pt, Ag, Ti, V and W,' Applied Optics **24**, 4493-99 (1985).

[17] C. Themistos, B. M. A. Rahman, M. Rajarajan, K. Kalli, and K. T. V. Grattan, 'Characterization of surface-plasmon modes in metal-clad optical waveguides,' Appl. Opt. **45**, 8523-8530 (2006).

[18] K. Saitoh and M. Koshiba 'Structural dependence of effective area and mode field diameter for holey fibers,' Opt. Exp. **11**, 1746-1756 (2003)
[19] A. Markelz, S. Whitmire, and J. Hillebrecht and R. Birge, 'THz time domain spectroscopy of biomolecular conformational modes,' Phys. Med. Biol. **47**, 3797–3805 (2002).
[20] P.H. Bolivar, M. Nagel, F. Richter, M. Brucherseifer1, H. Kurz, A. Bosserhoff and R. Buttner, 'Label-free THz sensing of genetic sequences: towards 'THz biochips',' Phil. Trans. R. Soc. Lond. A, **362** 323–335 (2004).